Chinese Chemical Letters 33 (2022) 4326–4330

Contents lists available at ScienceDirect

Chinese Chemical Letters

journal homepage: www.elsevier.com/locate/cclet

Polymerization-induced microphase separation of polymer-polyoxometalate nanocomposites for anhydrous solid state electrolytes

Lu Liu[a,1], Zicheng Wu[a,1], Zhao Zheng[a], Qianjie Zhou[a], Kun Chen[a,b,*], Panchao Yin[a,b,*]

[a] South China Advanced Institute for Soft Matter Science and Technology, School of Molecular Science and Engineering, South China University of Technology, Guangzhou 510640, China

[b] Guangdong Provincial Key Laboratory of Functional and Intelligent Hybrid Materials and Devices, South China University of Technology, Guangzhou 510640, China

ARTICLE INFO

Article history:
Received 11 November 2021
Revised 10 December 2021
Accepted 13 December 2021
Available online 17 December 2021

Keywords:
Solid-state electrolyte
Microphase separation
Bi-continuous structure
Polymer
Polyoxometalate

ABSTRACT

Solid-state electrolytes (SSEs) with high ionic conductivity, mechanical stability, and high thermal stability, as well as the stringent requirement of application in high-temperature fuel cells and lithium-ion batteries is receiving increasing attention. Polymer nanocomposites (PNCs), combining the advantages of inorganic materials with those of polymeric materials, offer numerous opportunities for SSEs design. In this work, we report a facile and general one-pot approach based on polymerization-induced microphase separation (PIMS) to generate PNCs with bi-continuous microphases. This synthetic strategy transforms a homogeneous liquid precursor consisting of polyoxometalates (POMs, $H_3PW_{12}O_{40}$, $Li_7[V_{15}O_{36}(CO_3)]$), poly(ethylene glycol) (PEG) macro-chain-transfer agent, styrene and divinylbenzene monomers, into a robust and transparent monolith. The resulting POMs are uniformly dispersed in the PEG block (PEG/POM) to form a conducting pathway that successfully realizes the effective transfer of protons and lithium ions, while the highly cross-linked polystyrene domains (P(S-*co*-DVB)) as mechanical support provide outstanding mechanical properties and thermal stability. As the POM loading ratio up to 35 wt%, the proton conductivity of nanocomposite reaches as high as 5.99×10^{-4} S/cm at 100 °C in anhydrous environment, which effectively promotes proton transfer under extreme environments. This study broadens the application of fuel cells and lithium-ion batteries in extreme environments.

Solid-state electrolytes (SSEs), as solid or quasi-solid materials with high ionic conductivities (IC), have emerged as high-priority materials for energy conversion and storage devices with promising safety and high energy density [1–6]. Generally, SSEs mainly include inorganic solid electrolytes (ISEs), solid polymer electrolytes (SPEs) and inorganic-organic hybrid composite electrolytes [7–9]. Dating back to 1960s, the discovery of the ceramic-based β-alumina and its successful application in Na-S batteries, bring the prelude to the ISEs system [10]. Nevertheless, they still suffer from several tough solid-solid interface compatibility issues resulting from their rigid nature [11]. SPEs represent a broad class of materials with long polymeric chains and relatively high ion concentrations that offer outstanding advantages over conventional liquid electrolytes in current lithium-ion batteries including no leakage of electrolytes, low flammability, good flexibility, safety and stable contact with the electrode [12,13]. SPEs possess excellent processability and flexibility as compared to ISEs, enabling their strong adhesive on the surface of electrodes and thus the decrease of interfacial impedance [14,15]. Especially, in fuel cells, reactants such as H_2 and O_2 and products such as H_2O continuously flow past the electrodes, and therefore, the effective polymer electrolyte membranes (PEMs) must maintain a combination of high modulus, toughness, stability, and high ionic conductivity [16–18]. However, the ionic conductivity in most SPEs is directly tied to segmental mobility and chain dynamics, which is difficult to improve along with mechanical strength simultaneously [19–22]. One way to accomplish this goal is the development of microphase separated polymers, wherein one of the microphases conducts ions while the other is responsible for the mechanical rigidity of the heterogeneous polymer electrolyte [23–

* Corresponding authors at: South China Advanced Institute for Soft Matter Science and Technology, School of Molecular Science and Engineering, South China University of Technology, Guangzhou 510640, China.

E-mail addresses: mschenk@scut.edu.cn (K. Chen), yinpc@scut.edu.cn (P. Yin).

[1] These authors contributed equally to this work.

https://doi.org/10.1016/j.cclet.2021.12.031
1001-8417/

26]. However, these protocols are complex, and much synthetic efforts are required. Although much progress has been made in fabricating microphase-separated structures, these strategies still require either relatively complex polymerization reactions or delicate modifications of nanoparticles (NPs). Therefore, there is an urgent need for general and cost-effective approaches for the design of SSEs with both promising conductivities and mechanical strengths.

Polymer nanocomposites (PNCs) are prepared by dispersing nano-sized inorganic phases into polymer matrix, which can lead to synergized functionalities better than the single component [27–30]. The PNCs combining the advantages of inorganic materials (for example, wide temperature range stability and high ionic conductivity) with those of polymeric materials (for example, strong plasticity and high processability) offer numerous opportunities for SSEs design [31–34]. Their application in PEMs is receiving increasing attention [18,35]. However, the bulk structures of PNCs are difficult to regulate as the interaction between the NP phases and polymers are complex and usually weak, leading to phase separation and the coagulation of NPs, and the long-term failure of PNC-based functional materials [33,36]. Polyoxometalates (POMs), as a large class of well-defined anionic molecular clusters of metal oxides with sizes at nanoscale [37], are widely used as inorganic building blocks to prepare functional hybrid materials, in particular POM-polymer composite electrolytes, owing to their high ionic conduction, excellent electrochemical stabilities, excellent thermal stability and electromagnetic response properties [38–40]. Zhang *et al.* developed a facile approach to fabricate bi-continuous polymer nanocomposites through a POM-induced phase transition of lamellar PS-*b*-P2VP [41]. The electrostatic cross-linking effect of POM on the P2VP chains contributes to the disturbance of the lamellar phase and the formation of a stable bi-continuous phase. Moreover, the POMs increase the proton conductivity of the system and endow the bi-continuous nanocomposites with an increased conductivity of 0.1 mS/cm and an enhanced Young's modulus of 7.4 GPa at room temperature. They also fabricate nanocomposite electrolytes containing inverse hexagonal cylindrical phase and highly ordered lamellar proton-conducting nanochannels, by the electrostatic self-assembly of a polyoxometalate $H_3PW_{12}O_{40}$ (PW_{12}) and other copolymers [42,43]. Recently, bi-continuous polymer composite electrolytes through the electrostatic self-assembly of PW_{12} and a comb copolymer PEEK-*g*-PVP have been reported with applications in the direct methanol fuel cells (DMFCs) [44]. Meanwhile, the introduction of nanomaterials with Li^+ conductive activity into polymers to prepare nanocomposite polymer electrolyte materials is also one of the important ideas for preparing lithium ion SPEs [1,4,11,12,19,20,24,34,45]. Herein, we report a facile and general approach for both proton and lithium ion conductive organic-inorganic nanocomposites for anhydrous SSEs. Nanocomposites with bi-continuous microphase separated structures are prepared using poly(ethylene glycol) (PEG) and cross-linked polystyrene (PS) block copolymers *via* polymerization-induced microphase separation (PIMS) [24–26,46]. The nanoscale molecular clusters of POMs are uniformly doped into the phase domain formed by the PEG block to constitute the conductive phase, while the cross-linked PS domain provides mechanical support and ensures the thermal and structural stability of SSEs. Specifically, reversible addition-fragmentation chain-transfer (RAFT) polymerization was implemented for the controlled growth of styrene and divinylbenzene (DVB) from a PEG macro-chain-transfer agent (PEG-CTA) in the presence of stoichiometric POMs. The POMs can effectively suppress the crystallization behavior of PEG blocks in nanocomposites and contribute to the effective segregation between the mechanical phases and conducting domains. PIMS nanocomposites make up the long-range, isotropic, cross-linked domains with an exceptional combination of ionic conductivity, thermal stability, and mechanical robustness, enabling them as promising candidates for high-temperature anhydrous PEMs applications.

Several POMs show high solubility in PEG melts, and herein, representative POMs with H^+ ($H_3PW_{12}O_{40}$, abbreviated as PW_{12}) or Li^+ ($Li_7[V_{15}O_{36}(CO_3)]\cdot ca.39H_2O$, abbreviated as V_{15}) as counterions, are dissolved with macromolecular initiator, PEG-CTA, and the obtained complexes are mixed with styrene monomers and crosslinking agent DVB for reversible addition- fragmentation chain-transfer (RAFT) polymerization (Figs. S1–S3, Tables S1 and S2 in Supporting information). Due to the incompatibility between PEG and styrene phase, the polymerization can induce the formation of bi-continuous microphases. POMs are uniformly dispersed in PEG phase region through hydrogen bonding (HB) and electrostatic interactions in nanocomposites while the cross-linked PS phase acts as a structural support skeleton (Fig. 1). It is reported in our previous work that sub-nm-scaled metal oxide cluster (PW_{12}) shows high solubility in the melt of PEG, fully inhibit the crystallization of PEG, and form stable nanocomposites with PEG, which facilitates the fast dynamics of PEG chains/segments, and the proton conduction in the PEG@POM hybrids by the diffusive motions of PEG chains [47]. The obtained PW_{12}-PEG5k-*b*-P(S-*co*-DVB) (PPBP) nanocomposites with variant POM contents (0, 10 wt%, 20 wt%, 30 wt%, 35 wt% PW_{12}) are abbreviated as PPBP0, PPBP10, PPBP20. PPBP30, PPBP35, respectively, showing promising proton conductivities at ambient conditions [48,49]. Meanwhile, the exploration of polyoxovanadate V_{15} as a cathode material for lithium ion batteries reveals its high current density and excellent cycling stability, which fully demonstrates the application prospects of V_{15} in solid-state lithium-ion batteries [26,45].

To investigate the internal structure of the nanocomposites, the materials are examined using small angle X-ray scattering (SAXS), wide angle X-ray scattering (WAXS), differential scanning calorimetry (DSC), and thermogravimetric analysis (TGA) techniques (Fig. 2). In general, a broad principal scattering peak at q^* and a weak higher order shoulder at about $2q^*$ in SAXS spectra are characteristic of a structured morphology with microphase-separated domains but without long-range periodic order [46]. The position of the primary scattering peak corresponds to the structural length scale of compositional heterogeneities ($d = 2\pi/q^*$), and the characteristic size between the PW_{12}/PEG and the P(S-*co*-DVB) domains is calculated to be 16–20 nm, significantly larger than the domain spacing between PEG and cross-linked PS phase (~12 nm) in samples without PW_{12}. The selective incorporation of the PW_{12} contributes to the volume fraction increasement of the conducting phase ($PEG + PW_{12}$) as well as the increasement of the effective interaction parameter, χ_{eff}, between the conducting phase and P(S-*co*-DVB) phase [50], leading to the increase in the average domain spacing between conducting phase and cross-linked PS phase (Fig. 2a) [51]. The increase of χ_{eff} leads to the increase of the phase separation strength and local order within the nanocomposites, as indicated by the appearance of a more pronounced shoulder at *ca.* $2q^*$ when POMs concentrations raise. Overall, the combination of PW_{12} and PEG domains forms the conductive phase, which enables the smooth conduction of protons, while the high modulus phase formed by the cross-linked PS domains provides the skeleton support for this material and ensure its high temperature resistance and mechanical stability in extreme environments.

Meanwhile, wide angle X-ray scattering (WAXS) technique is applied to detect the crystallization of PEG blocks in nanocomposites and the dispersion of POMs in PEG blocks (Fig. 2b). Because of the high sensitivity of X-ray to heavy metal ions, the form factor (P(Q)) corresponding to the morphology of PW_{12} molecular clusters and the structure factor (S(Q)) reflecting information such as interactions and possible aggregations between PW_{12} molecular clusters can be effectively collected using WAXS [52,53]. As

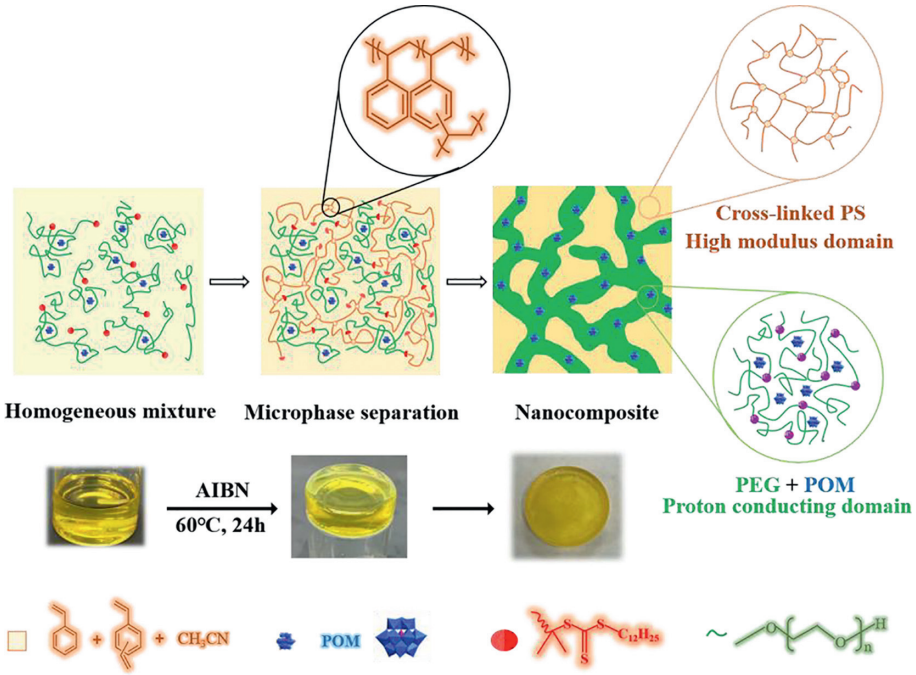

Fig. 1. Schematic preparation of anhydrous ionic conductive nanocomposite with microphase separation.

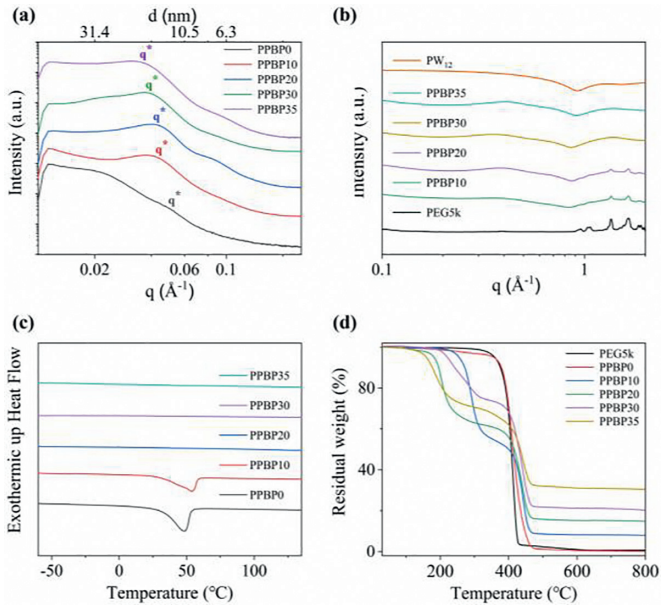

Fig. 2. Characterization of PW_{12}-PEG5k-*b*-P(S-*co*-DVB) (PPBP) PNCs with bi-continuous microphases prepared by polymerization-induced microphase separation (PIMS) approach: (a) SAXS, (b) WAXS, (c) DSC and (d) TGA curves of samples with variant PW_{12} content (0, 10 wt%, 20 wt%, 30 wt% PW_{12} for PPBP0, PPBP10, PPBP20, PPBP30, PPBP35, respectively).

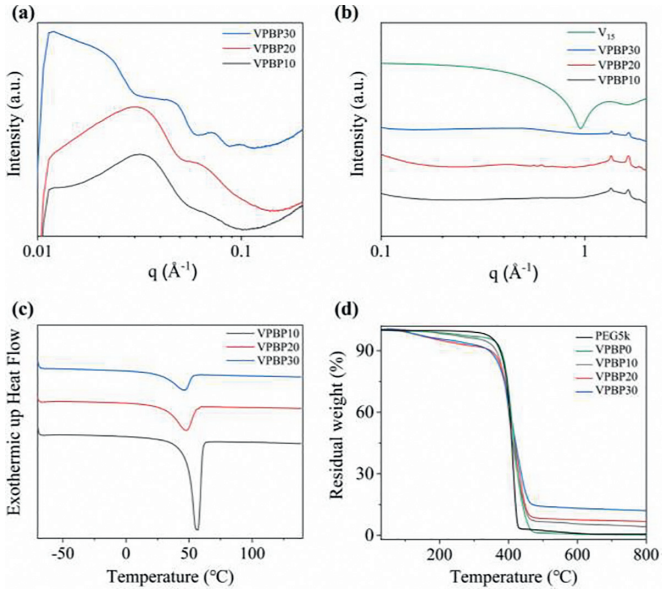

Fig. 3. Characterization of V_{15}-PEG5k-*b*-P(S-*co*-DVB) (VPBP) PNCs with bi-continuous microphases prepared by PIMS approach: (a) SAXS, (b) WAXS, (c) DSC and (d) TGA curves of the samples with variant V_{15} content (0, 10 wt%, 20 wt%, 30 wt% V_{15} for VPBP0, VPBP10, VPBP20, VPBP30, respectively).

shown in the wide-angle region of WAXS, POM clusters disperse homogeneously in PEG without aggregation and inhibit PEG crystallization completely even at high POM loadings. Owing to the strong interactions, PW_{12} clusters disperse in PEG to form stable complexes. Especially, in PW_{12}-PEG5k-*b*-P(S-*co*-DVB) nanocomposites with 35 wt% POM content (abbreviated as PPBP35), no obvious aggregated scattering peaks of POM can be observed. Form factor (P(Q)) and structure factor (S(Q)) of PW_{12} in PPBP35 nanocomposites together demonstrate the complete structure of PW_{12} and the uniform dispersity of PW_{12} in PEG blocks to form the final conductive phase [54]. These results consistent with the SAXS data described above.

Meanwhile, similar to PPBP, the microphase separated structure of the nanocomposites is maintained when the PW_{12} molecular clusters are changed to another POM V_{15}, suggesting the universality of this protocol for the preparation of microphase-separated nanocomposite electrolytes (Fig. 3). As shown in Fig. 3a, the same shape factor (P(Q)) corresponding to the morphology of the V_{15} molecular clusters can be observed in the V_{15}-PEG5k-*b*-P(S-*co*-DVB) (abbreviated as VPBP) nanocomposites, indicating the stability and well dispersion of the V_{15} clusters in the polymer matrix.

With the increase of V_{15} content, the crystalline scattering peaks of PEG blocks are gradually weakened, suggesting the role of V_{15} as inhibitor for the crystallization of PEG blocks (Fig. 3b).

Furthermore, the crystallization of PEG blocks in PPBP nanocomposites is quantitatively probed using DSC, and the roles of POMs for PEG crystallization inhibition can be revealed. At low PW_{12} content (0–10 wt%), an obvious crystalline melt peak can be observed around 50–60 °C, indicating that part of the PEG blocks in the nanocomposites are still in a crystalline state (Fig. 2c). When the mass ratios of PW_{12} increase to 20% or above, no obvious crystallization and melting process can be observed, indicating that POMs fully inhibit the crystallization of PEG blocks, which is consistent with the WAXS results. Similar crystallization inhibition effect can be observed in VPBP nanocomposites except that higher mass ratios of V_{15} is required for fully PEG crystallization inhibition (Fig. 3c).

The thermal stability of nanocomposites can be analyzed using TGA, and the TGA curves of nanocomposites with different POM contents are shown in Figs. 2d and 3d. It is often customary to use a characteristic temperature to illustrate the thermal stability of a material. The temperature at which the TGA curve begins to fall is called the starting decomposition temperature, the temperature at which the weight loss rate reaches 5% is called the decomposition 5% temperature, and the temperature at which the TGA curve begins to deviate from the baseline is called the extrapolation starting temperature. Because these temperature points are best reproduced, so these key temperature points are often used to characterize the thermal stability of materials. The temperature of 5% mass reduction of PEG5k-*b*-P(S-*co*-DVB) block copolymers without POMs appears at 300 °C, and the extrapolation onset temperature is even closer to 400 °C, indicating the high heat resistance of this copolymers. The thermal stability of the nanocomposites is slightly reduced after doping PW_{12}, but the temperature at 5% decomposition of the material and the extrapolation onset temperature are all above 200 °C, and the thermal stability is comparable to that of the phosphoric acid-doped benzimidazole high-temperature fuel cell electrolyte film [18]. The first weight loss plateau occurs due to the decomposition of parts of PEG blocks in the nanocomposites, and the second one is caused by the simultaneous decomposition of the cross-linked PS blocks with PW_{12} in the nanocomposites. At low PW_{12} content, the stability of the materials increases as the PW_{12} content increases. However, when the PW_{12} content reaches a certain level, the excess PW_{12} leads to a decrease in compatibility with the PEG blocks, resulting in a slight decrease in the overall stability of the material. Therefore, the doping content of nanomolecular clusters needs to be controlled in a suitable concentration range to achieve the optimal material properties.

At the same time, the thermal stability of VPBP nanocomposites is also observed by TGA. As shown in Fig. 3d, the addition of V_{15} shifts the starting decomposition temperature of the materials to a lower temperature, but the temperature at 5% decomposition of the sample mass and the extrapolation starting temperature are above 200 °C, indicating that the prepared VPBP nanocomposites have good heat resistance. However, unlike the PPBP nanocomposites, the weight loss curves of the VPBP samples do not show two plateaus, which also indicates that the interaction between V_{15} clusters and PEG blocks is greater than that between PW_{12} and PEG blocks. V_{15} clusters cause the decomposition of the entire block copolymers crosslinking network rather than decomposition of partial PEG decomposition first.

To measure the conductivity of microphase separated high-temperature anhydrous proton conductive nanocomposites, the typical electrochemical impedance spectroscopy (EIS) method is used to determine the ion conductivity of PPBP with different PW_{12} contents at different temperatures (Figs. 4a–c). The EIS spectra is fitted by ZSimpWin and $ZView_2$ software, and the proton conductivity of the nanocomposites can be calculated by using equation $\sigma = L/(R_bS)$ in combination with the actual dimensions of the samples. The calculated conductivities are summarized in Fig. 4d. With the increase of temperature, the increase of proton conductivity in the low temperature region (50–80 °C) is more obvious, because the crystallinity of PEG blocks in PPBP nanocomposites gradually decreases, and the chain movement of PEG blocks becomes fast, which promotes the proton conductivity. However, when the temperature rises to a high temperature above 100 °C, the dissociation of protons gradually reaches a maximum to the proton conductivity plateaus. The overall conductivity of PPBP nanocomposites is enhanced with the increase of PW_{12} content, as the addition of PW_{12} acts as an inhibitor to the crystallization of PEG blocks in this material, which in turn improves the proton conductivity of the prepared solid-state polymer electrolytes. The highest proton conductivity of 5.99×10^{-4} S/cm is achieved when the PW_{12} content is 35%, and the proton conductivity is maintained at a high level of 2.03×10^{-4} S/cm at 30% PW_{12} content under high temperature (150 °C) and anhydrous conditions, which confirms the ability of the nanocomposites in effectively proton transfer under extreme environments.

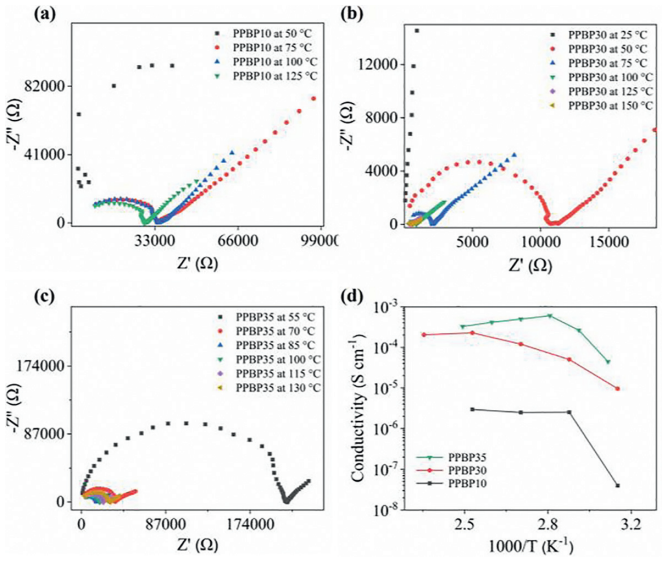

Fig. 4. (a–c) EIS spectra of PW_{12}-PEG5k-*b*-P(S-*co*-DVB) (PPBP) with (a) 10 wt%, (b) 30 wt% and (c) 35 wt% PW_{12} content (PPBP10, PPBP30, PPBP35, respectively) at different temperatures. (d) Temperature-dependent protonic conductivities of PPBP with various PW_{12} ratios (bottom up, 10 wt%, 30 wt%, 35 wt%).

Compared to the PPBP nanocomposites, VPBP have generally lower lithium ion conductivity (Fig. S4 in Supporting information), which is related to the size of Li^+ dissociated from V_{15} and the electronegativity of V_{15}. In the PEG conductive phase, the movement of Li^+ is more difficult than that of proton, so the conductivity is lower, but it can still indicate the feasibility and universality of this general approach to construct conductive nanocomposites using PEG, cross-linked PS block copolymers and POMs. At present, both positive and negative ions of lithium salts in PEG-based SSE materials can move, but this movement of negative ions in lithium ion batteries intensify the polarization within the materials, which will lead to an increase in the polarization voltage of the solid-state batteries. More severely, it will promote the growth of lithium crystal branches and pierce the battery to cause danger, so the lithium ion migration number (t_{Li^+}) is an important parameter used to evaluate the performance of SSEs [55]. Hence, VPBP30 nanocomposite was selected and tested at 80 °C using the potentiodynamic polarization method, and the chronoamperometry profiles and EIS spectra before and after polarization are shown in

Fig. S5 (Supporting information). The t_{Li^+} of the nanocomposites is calculated to be 0.87 by equation $t_{Li^+} = (I_s(\Delta V - I_0R_0))/(I_0(\Delta V - I_sR_s))$ that is similar to many reported single ion SSEs, indicating that the movement of V_{15} anion is restricted by strong electrostatic interactions with the PEG block, and the conductive process relies mainly on the movement of dissociated Li^+. Meanwhile, previous studies have shown that t_{Li^+} of PEG-based SSEs doped with lithium salt is about 0.2–0.3 because both positive and negative ions in the lithium salt can move [56–58]. Therefore, the doping of V_{15} raises the t_{Li^+} of PEG-based SSEs, which closes to that of single ion conductivity. The VPBP nanocomposites is expected to be used in solid-state lithium-ion batteries.

In summary, we present a facile, scalable, one-step synthetic protocol to fabricate high-temperature anhydrous conductive nanocomposites based on POMs and PEG5k-*b*-P(S-*co*-DVB) *via* polymerization-induced microphase separation. The POMs-PEG5k-*b*-P(S-*co*-DVB) nanocomposites exhibit a bi-continuous morphology, in which the POMs are uniformly dispersed in the PEG block (PEG/POM) to form a conducting pathway that successfully realizes the effective transportation of protons and lithium ions. The highly cross-linked PS domains (P(S-*co*-DVB)) serve as mechanical support and provide outstanding mechanical properties and thermal stability. The prepared nanocomposites overcome the safety and stability issues of conventional SSEs when working under high temperature conditions, and avoid the drawback that small molecules of acids in existing SSEs tend to leach out from the polymer matrix. Due to the broad availability of POMs and polymers with different functionalities, the SSE system can be facilely extended to a variety of functional electrolytes, *e.g.*, sodium-ion conductive electrolytes, which can extend the design of multifunctional SSE materials.

Declaration of competing interest

The authors declare that they have no known competing financial interests or personal relationships that could have appeared to influence the work reported in this paper.

Acknowledgments

The work is supported by National Natural Science Foundation of China (Nos. 21961142018, 22101086 and 51873067) and Natural Science Foundation of Guangdong Province (Nos. 2021A1515012024 and 2021A1515010271). We are grateful to BL16B1 of Shanghai Synchrotron Radiation Facility for the access to the synchrotron-based SAXS.

Supplementary materials

Supplementary material associated with this article can be found, in the online version, at doi:10.1016/j.cclet.2021.12.031.

References

[1] Y. Liu, P. He, H. Zhou, Adv. Energy Mater. 8 (2018) 1701602.
[2] K. Murata, S. Izuchi, Y. Yoshihisa, Electrochim. Acta 45 (2000) 1501–1508.
[3] Z. Gao, H. Sun, L. Fu, Y. Huang, et al., Adv. Mater. 30 (2018) 1705702.
[4] S. Ahmad, Ionics 15 (2009) 309–321.
[5] J. Shim, D.G. Kim, J.H. Lee, J.H. Baik, J.C. Lee, Polym. Chem. 5 (2014) 3432–3442.
[6] L. Yue, J. Ma, J. Zhang, et al., Energy Storage Mater. 5 (2016) 139–164.
[7] J. Janek, W.G. Zeier, Nat. Energy 1 (2016) 16141.
[8] F. Capuano, F. Croce, B. Scrosati, J. Electrochem. Soc. 138 (1991) 1918–1922.
[9] T. Ye, L. Li, Y. Zhang, Adv. Funct. Mater. 30 (2020) 2000077.
[10] L. Long, S. Wang, M. Xiao, Y. Meng, J. Mater. Chem. 4 (2016) 10038–10069.
[11] Y. Li, W. Zhou, S. Xin, et al., Angew. Chem. Int. Ed. 55 (2016) 9965–9968.
[12] J.B. Goodenough, K.S. Park, J. Am. Chem. Soc. 135 (2013) 1167–1176.
[13] Y. Kato, S. Hori, T. Saito, et al., Nat. Energy 1 (2016) 16030.
[14] A.M. Stephan, K.S. Nahm, Polymer 47 (2006) 5952–5964.
[15] G. Chen, L. Ye, K. Zhang, et al., Chem. Eng. J. 394 (2020) 124885.
[16] M.Y. Ghotbi, J. Mater. Sci. Mater. Electron. 30 (2019) 13835–13854.
[17] C. Meemuk, S. Chirachanchai, Fuel Cells 18 (2018) 181–188.
[18] M.B. Karimi, K. Hooshyari, P. Salarizadeh, et al., Int. J. Hydrog. Energy 46 (2021) 34413–34437.
[19] V. Bocharova, A.P. Sokolov, Macromolecules 53 (2020) 4141–4157.
[20] J. Mindemark, M.J. Lacey, T. Bowden, D. Brandell, Prog. Polym. Sci. 81 (2018) 114–143.
[21] K.S. Ngai, S. Ramesh, K. Ramesh, J.C. Juan, Ionics 22 (2016) 1259–1279.
[22] Y. Wang, F. Fan, A.L. Agapov, et al., Polymer 55 (2014) 4067–4076.
[23] D.T. Hallinan, N.P. Balsara, Ann. Rev. Mater. Res. 43 (2013) 503–525.
[24] S.A. Chopade, J.G. Au, Z. Li, et al., ACS Appl. Mater. Interfaces 9 (2017) 14561–14565.
[25] M.W. Schulze, L.D. McIntosh, M.A. Hillmyer, T.P. Lodge, Nano Lett. 14 (2014) 122–126.
[26] M. Zhang, A.M. Zhang, Y. Chen, et al., Energy Storage Mater. 29 (2020) 172–181.
[27] A.M. Díez-Pascual, Polymers 13 (2021) 2445.
[28] B.N. Tran, S.C. Thickett, V. Agarwal, P.B. Zetterlund, ACS Appl. Polym. Mater. 3 (2021) 5145–5154.
[29] C.I. Idumah, Synth. Met. 273 (2021) 116674.
[30] W.S. Tung, P.J. Griffin, J.S. Meth, et al., ACS Macro Lett. 5 (2016) 735–739.
[31] R. Zhao, Y. Wu, Z. Liang, et al., Energy Environ. Sci. 13 (2020) 2386–2403.
[32] L. Zhang, W. Du, A. Nautiyal, Z. Liu, X. Zhang, Sci. China Mater. 61 (2018) 303–352.
[33] L.M. Bronstein, C. Joo, R. Karlinsey, A. Ryder, J.W. Zwanziger, Chem. Mater. 13 (2001) 3678–3684.
[34] J. Wan, J. Xie, D.G. Mackanic, et al., Mater. Today Nano 4 (2018) 1–16.
[35] V. Di Noto, M. Bettiol, F. Bassetto, et al., Int. J. Hydrog. Energy 37 (2012) 6169–6181.
[36] J. Nanda, A. Biswas, B. Adhikari, A. Banerjee, Angew. Chem. Int. Ed. 52 (2013) 5041–5045.
[37] T. Liu, Langmuir 26 (2010) 9202–9213.
[38] P. Fan, H. Liu, V. Marosz, et al., Adv. Funct. Mater. 31 (2021) 2101380.
[39] L. Zhai, H. Li, Molecules 24 (2019) 3425.
[40] N. Ogiwara, M. Tomoda, S. Miyazaki, et al., Nanoscale 13 (2021) 8049–8057.
[41] L. Zhang, T. Cui, X. Cao, et al., Angew. Chem. Int. Ed. 56 (2017) 9013–9017.
[42] L. Zhai, S. Chai, G. Wang, et al., Macromol. Rapid Commun. 41 (2020) 2000438.
[43] H. He, G. Wang, S. Chai, et al., Chin. Chem. Lett. 32 (2021) 2013–2016.
[44] G. Wang, J. Li, L. Shang, et al., CCS Chem. 3 (2021) 603–613.
[45] J. Chen, M. Symes, S. Fan, et al., Adv. Mater. 27 (2015) 4649–4654.
[46] M. Seo, A.H. Marc, Science 336 (2012) 1422–1425.
[47] H. Wu, L. Li, M. Tsuboi, et al., J. Phys. Chem. Lett. 9 (2018) 5772–5777.
[48] Z. Zheng, Q. Zhou, M. Li, P. Yin, Chem. Sci. 10 (2019) 7333–7339.
[49] Z. Zheng, M. Li, Q. Zhou, et al., ACS Appl. Nano Mater. 4 (2021) 811–819.
[50] W.S. Young, T.H. Epps, Macromolecules 42 (2009) 2672–2678.
[51] T.P. Lodge, B. Pudil, K.J. Hanley, Macromolecules 35 (2002) 4707–4717.
[52] P. Yin, B. Wu, T. Li, et al., J. Am. Chem. Soc. 138 (2016) 10623–10629.
[53] P. Yin, B. Wu, E. Mamontov, et al., J. Am. Chem. Soc. 138 (2016) 2638–2643.
[54] P. Lindner, T. Zemb, Mater. Today 5 (2002) 38.
[55] J. Evans, C.A. Vincent, P.G. Bruce, Polymer 28 (1987) 2324–2328.
[56] R. Fan, C. Liu, K. He, et al., ACS Appl. Mater. Interfaces 12 (2020) 7222–7231.
[57] J.P. Donoso, L.V.S. Lopes, A. Pawlicka, et al., Electrochim. Acta 53 (2007) 1455–1460.
[58] Z. Xiao, B. Zhou, J. Wang, et al., J. Membr. Sci. 576 (2019) 182–189.